frontiers | Frontiers in Earth Science

TYPE Original Research
PUBLISHED 09 January 2023
DOI 10.3389/feart.2022.1075941

OPEN ACCESS

EDITED BY
Chen Zhang,
Chengdu University of Technology, China

REVIEWED BY
Xiaojie Geng,
China University of Geosciences, China
Wei Wu,
Henan Polytechnic University, China

*CORRESPONDENCE
Hui Zhou,
zhouhui03@petrochina.com.cn

†These authors have contributed equally to this work and share first authorship

SPECIALTY SECTION
This article was submitted to Economic Geology, a section of the journal Frontiers in Earth Science

RECEIVED 21 October 2022
ACCEPTED 15 November 2022
PUBLISHED 09 January 2023

CITATION
Zhou H, Gao D, Huang L, Zhu G, Zhang T, Liu J, Zhai X, Xiong R, Wang S and Zhang Y (2023), Characteristics and genesis of dolomite in the lower Cambrian Xiaoerbulake Formation of the western Tarim Basin, China. *Front. Earth Sci.* 10:1075941. doi: 10.3389/feart.2022.1075941

Characteristics and genesis of dolomite in the lower Cambrian Xiaoerbulake Formation of the western Tarim Basin, China

Hui Zhou[1*†], Da Gao[2†], Lili Huang[3], Guangyou Zhu[1], Tianfu Zhang[3], Jingjiang Liu[1], Xiufen Zhai[1], Ran Xiong[3], Shan Wang[1] and Yuanyin Zhang[4]

[1]Research Institute of Petroleum Exploration and Development, PetroChina, Beijing, China, [2]School of Geosciences, Yangtze University, Wuhan, China, [3]Hangzhou Institute of Geology, PetroChina, Hangzhou, China, [4]Oil and Gas Survey Center of China Geological Survey, Beijing, China

The Lower Cambrian Xiaoerbulake Formation consist of thick dolostones which are high-quality hydrocarbon reservoir in the western Tarim Basin, but the origin of dolomite is still controversial, which lead to poor understanding to the origin of reservoir beds. By using the latest core data of Well XKD-1, we analyzed the petrology and geochemistry of the formation in order to clarify the genesis of dolomite. The geochemical analysis includes Sr, C, and O isotopes, and *in-situ* minor element and rare Earth element measurements for different types of dolomites by laser ablation inductively coupled plasma mass spectrometry (LA-ICP-MS). Four types of lithofacies are recognized in the Xiaoerbulake Formation based on different textures, which are laminated dolostone, thrombolite dolostone, bacteria-bonded dolostone, and grain dolostone. Two types of dolomites can be separated which are matrix dolomite (MD) and cement dolomite (CD). MD is the primary type of laminated and bacteria-bonded dolostone, and CD was developed mainly in grain dolostone and thrombolite dolostone. The $\delta^{13}C$ and $\delta^{18}O$ indicate that the grain dolostone and thrombolite dolostone have undergone more intensive diagenetic modification. On the contrary, the diagenetic modification of laminated and bacteria-bonded dolostone are relatively weak, which implies that the dolomitization of the latter two lithofacies occurs before burial stage. The $^{87}Sr/^{86}Sr$ ratio indicates that the corresponding fluid for dolomitization was seawater or marine-origin fluids. The MD was formed in the near-surface stage *via* the penecontemporaneous dolomitization of seawater or hyper-saline seawater. The dolomitization of CD occurred in the burial environment with the porosity was filled by marine-origin fluid, indicating a seepage-reflux dolomitization process. Both types of dolomites are partially affected by hydrothermal activities.

KEYWORDS

dolomitization, dolomite genesis, *in-situ* geochemical test, carbonate reservoir, Cambrian, Tarim Basin

1 Introduction

Dolomite rocks were widely distributed in the ancient stratigraphic record and comprise a large portion of the World's hydrocarbon and thus have been the focus of long-term research interest. Dolomitization can occur in diverse geological environment and timing, and the formation of dolomite is affected by many factors, such as sedimentary environment, diagenetic process, tectonic settings, and hydrological condition (Zenger et al., 1980; Warren, 2000). In the past few decades, considerable and various models were proposed for the process of dolomitization, however the origin of continuous series of dolomites in ancient times is still a mystery. Hydrocarbon exploration confirmed that dolomite presents better porosity and permeability and thus a higher value of exploration compared with limestone when they have similar burial depth (He et al., 2014; Gao et al., 2021a). Determining the genesis of dolomite and dolomitization process are important for better understanding the genesis reservoir rocks (He et al., 2014; Zhu et al., 2019; Liu et al., 2020).

As the hydrocarbon exploration in deep and ultra-deep carbonate rocks became one of the major trends in China these years (He et al., 2014; Gao et al., 2021b), increasing attention has been paid to the Cambrian pre-salt dolomite in the Bachu area, western Tarim Basin (Wang et al., 2014; Yang et al., 2020). As a result, wells He-4, Shutan-1, Kang-2, Mabei-1, and Batan-5 explored high-quality reservoir beds and oil and gas flow in the Lower Cambrian Xiaoerbulake Formation (Yan et al., 2017). The genesis of the dolomite reservoir thus became a research focus. Li et al. (2017) found that the Xiaoerbulake Formation in the Bachu area mainly developed the silty-fine crystalline dolomite and micritic-micro crystalline dolomite, which were mostly attributed to burial dolomitization, evaporation pump and seepage reflux dolomitization in local areas, and somewhat hydrothermal activities. Zhang et al. (2021) claimed that the Xiaoerbulake Formation reservoirs of Well Shutan-1 were dominated by the burial dolomitization, and to some extent affected by hydrothermal activities. Bai et al. (2021) stated that the early diagenetic microbial, evaporation pump and seepage reflux dolomitization lay down the basis for the development of the storage space of the Lower Cambrian dolomite of the Aksu outcrop, the northwestern Tarim Basin. Inconsistent understanding of dolomitization leads to dispute on reservoir origin, mostly because the geochemical analyses of the above studies failed to distinguish different types of dolomites with distinct fabrics and thus cannot accurately determine dolomitization process.

In this research, different types of dolomites are distinguished based on the lithofacies analysis, using the latest scientific drilling data of the western margin of the Tarim Basin.

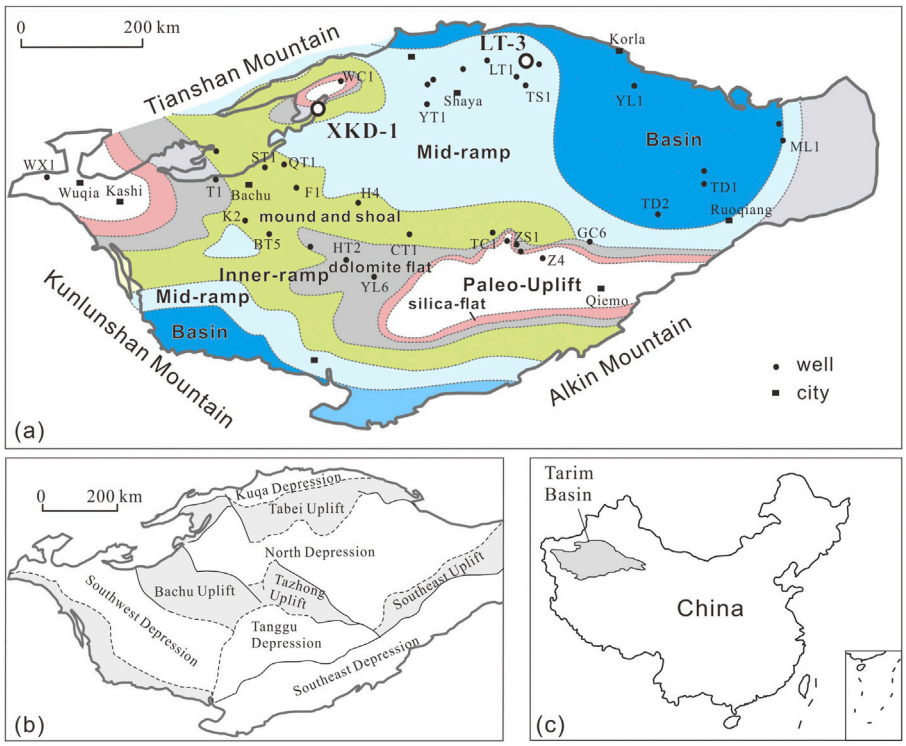

FIGURE 1
Lithography paleography during the deposition of the Xiaoerbulake Formation (modified from Wei et al., 2021) and the location of well XKD-1. **(A)** Lithography paleography of the Xiaoerbulake Formation. **(B)** Tectonic units of the Tarim Basin. **(C)** The location of the Tarim Basin.

The geochemical data of major elements, minor elements, and rare Earth elements of different dolomite in the Xiaoerbulake Formation were obtained using LA-ICP-MS, which sufficiently avoids the possible sample mixing and pollution in the case of bulk-rock analysis. This research is meaningful for sourcing dolomitizing fluids, clarifying the dolomitization process, and subsequently, determining the genesis of favorable reservoirs.

2 Geological setting

The Tarim Basin can be divided into three uplifts and four depressions which are the Tabei Uplift (North Tarim), Central Uplift, Tanan Uplift (South Tarim), Kuqa Depression, Northern Depression, Southwestern Depression, and Southeastern Depression (Figure 1). The wells and outcrops used in this research are mainly located in the Tabei and Central Uplifts, where the Cambrian is composed of, from bottom to top, the Lower Cambrian Yuertusi, Xiaoerbulake, and Wusonggeer Formations, the Middle Cambrian Shayilike and Awatage Formations, and the Upper Cambrian Qiulitage Formation. A parallel unconformity separates the Yuertusi Formation and the underlying Sinian strata, while other strata are in conformable contact with each other (Yan et al., 2017). The Tarim Basin experienced intensive Neoproterozoic stretching, which led to series of northeast-trending rifts in the southwestern Tarim. Meantime, the rifts of the northeastern and northwestern Tarim might be connected to the rifts (Ren et al., 2017; Guan et al., 2018). During the Early Cambrian, the Southern Tianshan Ocean in the northern basin was gradually expanded, and the basin was generally within weak stretching and subsidence and presented the characteristics of a passive continental margin basin (Yan et al., 2018). At that time, the basin was characterized by the development of shallow carbonate ramp, and the northeastern basin was dominated by deep-water basin filled by thick siliceous and calcareous mudstone (Zhu et al., 2019).

The Xiaoerbulake Formation (c.a.521~515 Ma) is in conformable contact with both the underlying Yuertusi Formation and the overlying Middle Cambrian Wusonggeer Formation (Figure 2). The west Tarim Basin generally showed a sedimentary evolution process from basin to carbonate ramp, then to carbonate platform during the early Cambrian (Song et al., 2020; Ouyang et al., 2022). The Yuertusi Formation is mainly composed by dark and thin-bedded shales interbedded with chert in the lower part, and limestones and dolostones with minor shales in the upper part, representing a transition from outer-ramp and basin to middle ramp (Ouyang et al., 2022). The field research in the Keping area shows that the Xiaoerbulake Formation can be divided into two members. The lower member is characterized by laminar microbial dolomite deposited in a carbonate middle-to outer-ramp. The upper member is characterized by clotted and stromatolite microbial dolomite, micritic dolomite, and granular dolomite indicating a carbonate platform (Song et al., 2014; Huang et al., 2015; Song et al., 2020). The thickness of Xiaoerbulake Formation is mostly 80–120 m in the west part of the basin, and some area up to 200 m (Zhang et al., 2021).

3 Materials and methods

After sedimentary description of the cores of the lower Cambrian Xiaoerbulake Formation in Well XKD-1 and Well LT-3, we collected 66 samples (64 from Well XDK-1, and 2 from Well LT-3) for further research. We first prepared 66 thin sections (~30 μm thick) with alizarin red S and potassium ferricyanide stained. The petrographic analysis was performed using the polarizing microscope (Leica DM4P) in the experiment center of the College of Earth Sciences, Yangtze University.

We further selected 18 samples of Well XKD-1 for isotope analysis after petrographic study. We used a handful micro-drill to grind the sample and obtained 200 mg of powder for each sample. The drilled hole was designed to avoid positions with fractures, dissolution pores, and intensive diagenetic alteration. 100 mg of samples were used for carbon and oxygen isotope analysis and the other 100 mg for the strontium isotope analysis.

The carbon and oxygen isotope analysis were carried out in the experimental center of the College of Earth Sciences, Yangtze University, using the Delta V Advantage gas isotope ratio mass spectrometer manufactured by Thermo Fisher Scientific (Germany). The test method was the phosphoric acid method, in which the sample reacts with 100% phosphoric acid at (25 ± 0.1)^{o}C for 24 h under the high vacuum condition. Then, the collected CO_2 was input to the MAT-252 stable isotope gas mass spectrometer for carbon and oxygen isotope ratio determination. The reference material used in the test was the IAEA-CO-8 calcite, and the test results were based on the PDB standard. The test error of carbon isotopes was 0.022‰ and that of oxygen isotopes was 0.035‰.

The strontium isotope analysis was carried out in the test center of the PetroChina Hangzhou Research Institute of Geology, using the TRITON Plus thermal ionization isotope ratio mass spectrometer. The reference material was the Gbw04411 standard sample. The ambient temperature for tests was 22°C and the ambient humidity was 62% RH. The test conditions were described below: The ionization temperature was over 1250°C; the ion source vacuum degree was less than 3×10^{-7} Mba; the sample particle size (Ø) was no larger than 0.075 mm. The test accuracy was less than 0.01%. The data processing software was Thermo Tune.

We selected additional six samples (5 of Well XKD-1 and 1 of Well Lt-3) to prepare ~60 μm-thick thin sections for major and minor elements (including rare Earth elements

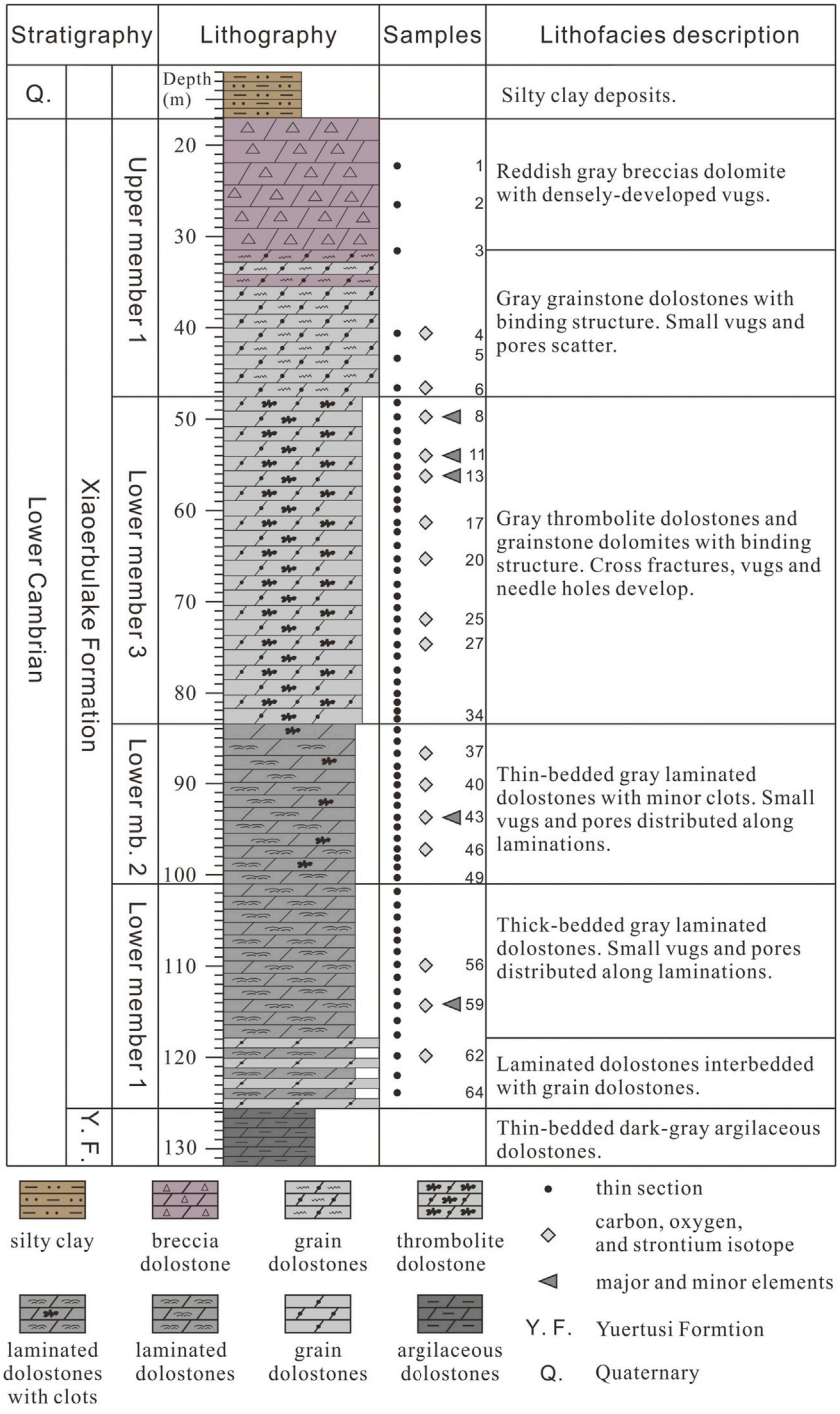

FIGURE 2
Comprehensive stratigraphic column of Well XKD-1.

and yttrium). The tests were completed in Wuhan SampleSolution Analytical Technology Co., Ltd. using laser ablation inductively coupled plasma mass spectrometer (LA-ICP-MS). For details of the instrument parameters and test procedures, please refer to Zong et al. (2017). The GeolasPro laser ablation system consists of the COMPexPro 102 ArF 193 nm excimer laser and MicroLas optical system. The ICP-MS instrument model is Agilent

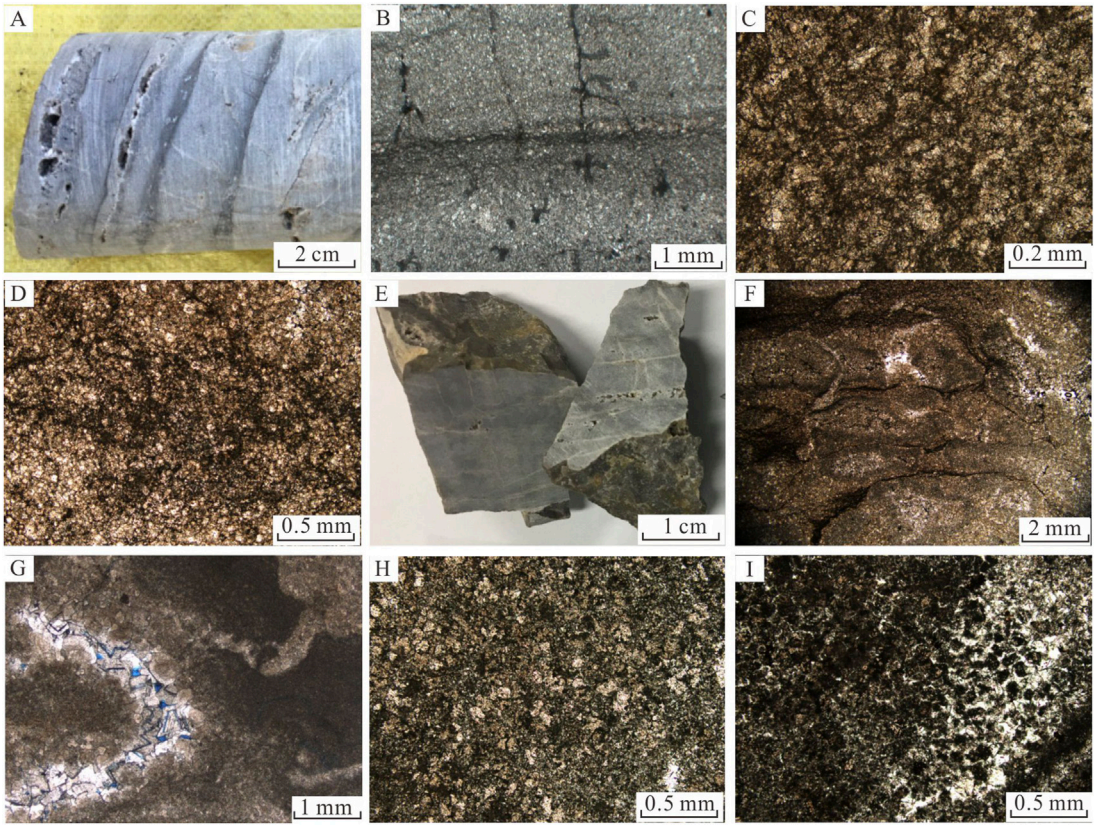

FIGURE 3
Main types of lithofacies of the Xiaoerbulake Formation in well XKD-1 **(A).** Laminated dolostone, 112 m; **(B)**. The clear laminated structure, mainly composed of micritic-silty dolomite, 95.2 m, sample XKD1-44; **(C)**. Bacteria-bonded dolostone, mainly composed of micritic-silty dolomite, with a dark network bacteria-bonded structure, 58.8 m, sample XKD1-13; **(D)**. Bacteria-bonded dolostone, mainly composed of micritic-silty dolomite, with a dark lumpy bacteria-bonded structure, 70.1 m, sample XKD1-21; **(E)**. Thrombolite dolostone, with dark clots unevenly distributed, 96.6 m; **(F)**. Thrombolite dolostone, internally composed of dark micrites and with the unclear boundary, 57.2 m, sample XKD1-11; **(G)**. Thrombolite dolostone, with dark irregular bacterial lumps, cement dolomite filling among these lumps, and a few residual pores, sample XKD1-22; **(H)**. Grain dolostone with an unclear bacteria-bonded structure, 44.4 m, sample XKD1-4; **(I)**. Grain dolostone with an unclear bacteria-bonded structure, 45.3 m, sample XKD1-5.

7700e. In the process of laser ablation, helium was used as the carrier gas, and argon, as the compensation gas to adjust the sensitivity, which were mixed through a T-joint before entering the ICP. The laser ablation system was equipped with a signal smoothing device (Hu et al., 2015). The laser beam width and frequency in this analysis were 44 μm and 50 Hz, respectively. The calculation of the content of trace elements of a single mineral, the calibration featuring multi-external standards with no internal standard was carried out using three USGS glasses of BHVO-2G, BCR-2G, and BIR-1G (Liu et al., 2008). Each time-resolved analysis data included a blank signal of about 20–30 s and a sample signal of about 50 s. The offline processing of test data (including the extraction of sample and blank signals, drift correction of instrument sensitivity, and element content calculation) were completed using the software ICPMSDataCal (Liu et al., 2008).

With the LA-ICP-MS, we analyzed a total of 44 test points covering different types of dolomites. In view of the factors such as the pollution of sample points by terrestrial clasts, acquisition degree of rare Earth elements, and data quality, 24 sample points were selected for analysis, and the rare Earth elements were PAAS-normalized.

4 Petrological and mineralogical characteristics of dolomite

4.1 Dolostone lithofacies

The Xiaoerbulake Formation in Well XKD-1 is mainly composed of five types of lithofacies which are laminated dolostone, bacteria-bonded dolostone, grain dolostone, thrombolite dolostone, and breccia dolostone (Figure 3).

4.1.1 Laminated dolostone

Gray and light-gray laminated dolostones widely developed in the lower part of the Xiaoerbulake Formation of Well XKD-1 (Figure 2). The lamina are several millimeters thick with wavy morphology (Figure 3A). Under the microscope, the rock matrix is mainly composed of micritic to silt-sized dolomite, mostly subhedral with dull surfaces (Figure 3B). The stylolites filled by dark asphalt are common. Pores developing along laminae are mostly at the millimeter-centimeter scale and show different degrees of filling. The boundaries of these pores are surrounded by fine-medium dolomite, which is also euhedral. Some pores are filled by blocky calcite. The visual porosity at the bottom is about 0.5%–2%, which increases to 2%–8% vertically upward.

4.1.2 Bacteria-bonded dolostone

Bacteria-bonded dolostones frequently developed in the Lower Member of Xiaoerbulake Formation of Well XKD-1, and mainly alternate with laminated and thrombolite dolostone (Figure 2). They mostly show gray-to dark gray color without laminated structure. Moreover, the bacteria-bonded dolostone primarily consists of micritic-silty dolomite, which is mostly subhedral and relatively dull. Dark flocculent and network micrites with abundant organic matter commonly developed to different degrees (Figures 3C,D). A small proportion of silt-sized and clean dolomites are scattered in dark micritic dolomite. Only a few inter-crystalline pores are found in the silty dolomite and the visual porosity is generally less than 1%.

4.1.3 Thrombolite dolostone

Thrombolite dolostone mainly developed in the upper part of the Lower Member of the Xiaoerbulake Formation of Well XKD-1, with a thickness of 36 m (Figure 2). It is generally gray and characterized by dark-gray irregular patches distributed in the light-gray matrix (Figure 3E). The dark clots are composed of micrites and fine peloids (Figure 3F, 3G). Dark flocculent and network components in the micrites indicate microbially-induced precipitation with rich organic contents. The clots are leaf-shaped, and sparry cements between them includes euhedral dolomite and blocky calcite. Reticular fractures developed in thrombolite dolostone, and mostly filled with dolomite and calcite cements. The visual porosity is about 2%–6%.

4.1.4 Grain dolostone

Grain dolostone mainly occur in the Upper Member of the Xiaoerbulake Formation of Well XKD-1 and associated with the thrombolite dolostones (Figure 2). They are commonly light gray in color and show massive structure. The grains are mostly silt-sized (0.05–0.1 mm), dark gray, and well-sorted peloids which densely distributed (Figure 3H, 3I). Unclear bacteria-bonded structures are found between the grains and mainly consists of subhedral-anhedral micritic-silty dolomite. The pores of grain dolostone are mainly inter-crystalline pores and vugs with a diameter of millimeters to a few centimeters. Most pores remain open and the visual porosity is about 5%–8%.

4.1.5 Breccia dolostone

Breccia dolostone, mostly light pink to gray, mainly developed in the uppermost part of the Xiaoerbulake Formation of well XKD-1 (Figure 2). This section is characterized by high-angle fractures and vugs with different sizes. The primary rocks were mainly bacteria-bonded dolostones and grain dolostones. The vugs are mostly centimeter-sized, with a few up to 5 cm. The visual porosity is about 5%–15%. This section is overlain by the Quaternary deposits.

4.2 Dolomite types

Based on the petrographic analysis, the dolomite in the Xiaoerbulake Formation can be divided into two types which are matrix dolomite (MD) and cement dolomite (CD).

4.2.1 Matrix dolomite

Matrix dolomite is characterized by silt-sized (0.01–0.1 mm) and subhedral crystals that extensively developed in all lithofacies. Most crystals of MD are cloudy and some larger ones have clear rims. In bacteria-bonded dolostone and thrombolite dolostone, bacteria-bonded structures were preserved in this type of dolomite. The lithofacies and mineralogical characteristics of this dolomite indicate the penecontemporaneous dolomitization.

4.2.2 Cement dolomite

Cement dolomite has larger crystals (0.1–0.5 mm) that are mainly euhedral, bright and clean filling in pores and vugs. Some crystals present clear rims and zonation indicating multi-stage growth. Most pores and vugs are partially filled with CD leaving effective porosity. In some pore-vugs, CD is associated with the later infilled coarse blocky calcite cement (BC).

5 Geochemical characteristics

5.1 Carbon and oxygen isotopes

The cross plot of carbon and oxygen isotope of these samples is shown in Figure 4 $\delta^{13}C$ of the 18 samples ranges from 0.873‰ to 3.097‰ V_{PDB} and $\delta^{18}O$ from -11.201‰ to -9.321‰V_{PDB}. The average $\delta^{13}C$ (2.601‰ V_{PDB}) and $\delta^{18}O$ (-9.516‰ V_{PDB}) of the limestone samples of Well LT-3 are slightly higher than the overall average values. The average $\delta^{13}C$ of the bacteria-bonded and laminated dolostone lithofacies are close to each other, but their data points are far deviated from those of the clotted and grain dolostone, which is shown by the generally depleted $\delta^{18}O$

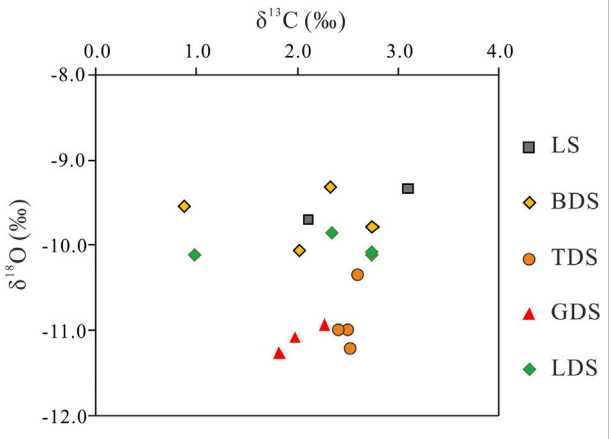

FIGURE 4
The cross-plot of carbon and oxygen isotope for different types of lithofacies in the Xiaoerbulake Formation.

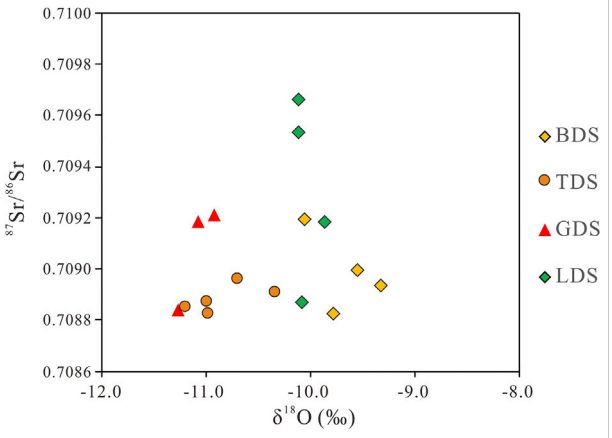

FIGURE 5
The cross-plot of strontium and oxygen isotope for different types of lithofacies in the Xiaoerbulake Formation.

(from -10.114‰ to -9.321‰ V_{PDB}). The scattered points of thrombolite dolostone and grain dolostone are also far separated and $\delta^{13}C$ of the former (2.532‰ V_{PDB}) is slightly enriched than that of the latter (2.019‰ V_{PDB}).

5.2 Strontium isotopes

Measurement of strontium isotope ratios of the 16 XKD-1 dolomite samples (Figure 5) show that the $^{87}Sr/^{86}Sr$ ratio ranges from 0.0708824 to 0.709661, averaging 0.709054. The $^{87}Sr/^{86}Sr$ values of different lithofacies are very close. Two laminated dolostone (LDS) samples yields slightly higher $^{87}Sr/^{86}Sr$ ratios

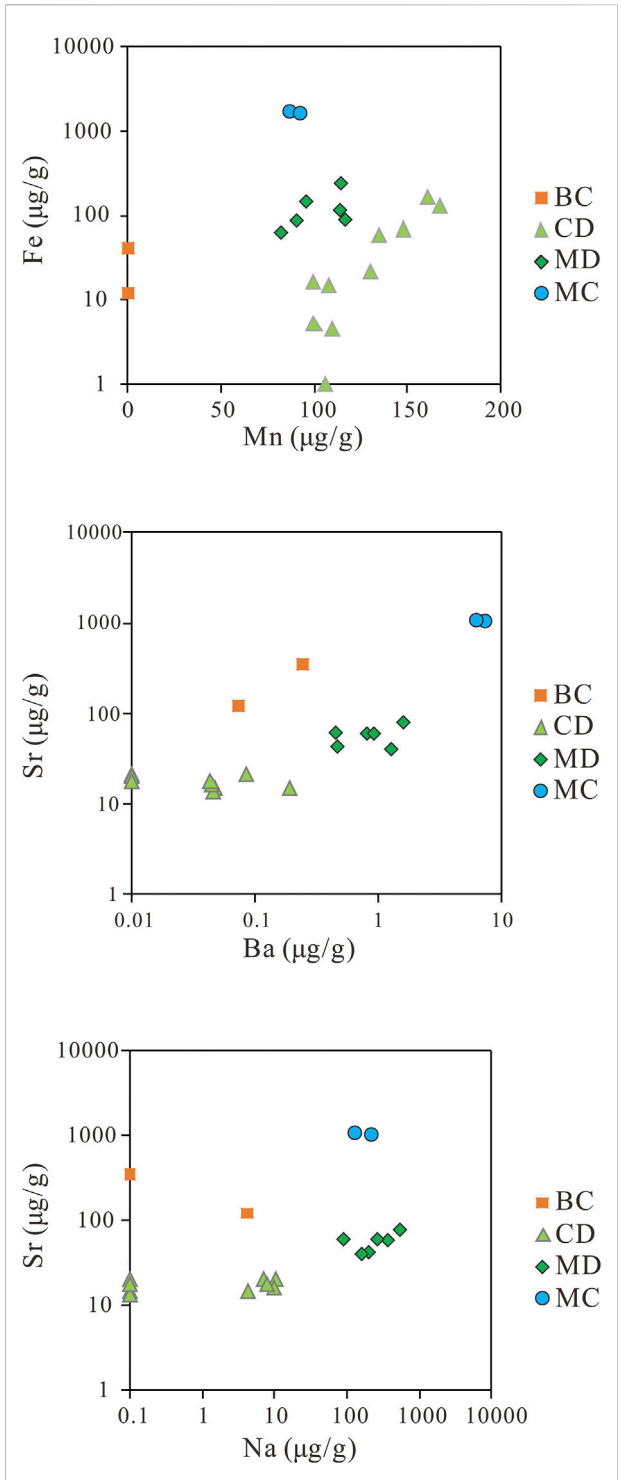

FIGURE 6
The cross-plots of major and minor elements of different types of dolomites in the Xiaoerbulake Formation of well XKD-1.

(0.709533 and 0.709661, respectively) than the average, while the thrombolite dolostones have slightly lower $^{87}Sr/^{86}Sr$ ratios (ranging from 0.708829 to 0.708964) than the average.

5.3 Major and minor elements

Six samples were analyzed for Si, Ti, Zr, Fe, Mn, Sr, Ba, and Na (Table 1). The scatter points of the two types of dolomites (MD and CD), micrite calcite (MC) and blocky calcite cement (BC) are separated from each other in the cross plots (Figure 6).

Compared with two dolomite types (MD and CD) and BC, MC in micrite limestone of Well LT-3 presents significantly higher content of Sr, Ti, Zr, Si, Fe, and Ba. The MD has Fe contents ranging from 44.505 to 242.093 μg/g (averaging 111.401 μg/g), Mn contents 73.965–119.788 μg/g (averaging 99.470 μg/g). The Fe contents of CD is lower (0–164.243 μg/g, averaging 52.001 μg/g), while the Mn content is slightly higher (94.089–167.411 μg/g, averaging 120.879 μg/g), compared with those of matrix dolomite. The MC has the highest Fe content (averaging 1683.781 μg/g), and Mn content close to the average value of MD. The Fe and Mn contents of the BC are extremely low, ranging from 12.030 μg/g to 46.558 μg/g (averaging 26.904 μg/g) and 0–1.396 μg/g respectively.

The MD have higher Na contents (89.701–802.925 μg/g, averaging 282.879 μg/g) than the CD samples ranging from 0 to 12.778 μg/g (averaging 4.274 μg/g). The Sr content of MD is 36.345–91.539 μg/g (with an average of 55.354 μg/g), while that of cement dolomite CD is slightly lower, ranging from 13.558 μg/g to 35.389 μg/g (averaging 18.998 μg/g). The MC presents the Na content (1036.438 μg/g) similar to that of MD, and yet significantly higher Sr content (1076.113 μg/g). The Sr content in the BC is close to that of the matrix dolomite MD, but the Na content is greatly lower, ranging from 0 to 4.240 μg/g (averaging 1.415 μg/g). The scatter plot of Sr versus Na (Figure 6) shows noted difference between the matrix dolomites and cement dolomites.

The scatter plot of Sr versus Ba (Figure 6) also shows that MD having significantly higher Ba contents than the CD. The Ba contents of MD range from 0.453 μg/g to 2.091 μg/g (averaging 0.943 μg/g), and that of CD ranges from 0 to 0.190 μg/g (averaging 0.038 μg/g). The MC has the highest Sr and Ba values, while the Ba content of BC is similar to that of CD.

5.4 Rare Earth elements and yttrium

The rare Earth element (REE) contents of the two types of dolomites are presented in Table 2. ΣREE + Y of CD range from 0.268 μg/g to 0.924 μg/g (averaging 0.512 μg/g), slightly higher than that of matrix dolomite MD (0.160 μg/g to 0.236 μg/g, averaging 0.186 μg/g). The MC has the highest ΣREE + Y. With respect to the REE + Y pattern (Figures 7, 8), the MD mainly presents a slightly left-leaning pattern, and some samples with depleted HREE, which results in a hat-like enrichment pattern. The CD has the similar pattern as MD, but the CD shows feature of enriched MREE and depletion of both LREE and HREE. The REE + Y of MC shows flat pattern with a slight depleted HREE. The BC also presents a slightly left-leaning pattern with a relative depletion of Yb and Lu.

The Pr/Yb ratios of dolomites and calcites vary considerably (Figure 9). The Pr/Yb of MD vary from 0.373 to 2.043, with an average of 0.963; that of CD is 0.442–1.456, with an average of 0.750. This means that both types of dolomites are characterized by depletion of LREE, and the CD has more significant depletion of LREE than MD.

Ce/Ce* of different types of dolomites also vary (Figure 9). MD has a negative Ce anomaly (0.49–0.89, averaging 0.70), while CD has a slight negative Ce anomaly (0.75–1.07, averaging 0.93). BC has a intense negative Ce anomaly (0.01 and 0.05), while MC presents no Ce anomaly (0.96 and 1.00).

The overall Eu/Eu* ranges from 0.593 to 2.290 (average 1.213) (Figure 9). The MD shows a negative Eu anomaly for three samples, and positive anomalies for two samples. The Eu/Eu* distribution of cement dolomite ranges from 0.625 to 2.215 (average 1.195). Moreover, for CD, half of the samples display positive Eu anomalies, while the other half display negative anomalies. The Eu/Eu* of two samples of blocky calcite are 0.563 and 2.569, respectively.

The Y/Ho ratios of different components are greatly varied. The Y/Ho of MD ranges from 21.70 to 55.77 (average 40.38), CD from 26.20 to 83.17 (average 55.40), BC from 30.70 to 31.11 and MC from 52.19 to 165.28.

6 Discussion

6.1 Sedimentary environments

Studies on the lithofacies paleo-geography of the Early Cambrian in the Tarim Basin found that the sedimentary environment at the west part of the basin is characteristic by a carbonate ramp or restricted platform during the deposition of the Xiaoerbulake Formation, and the distribution of lithofacies is controlled by tides, water circulation, water depth, and paleo-geomorphology (Huang et al., 2014; Song et al., 2020; Zheng et al., 2020; Zheng et al., 2020; Gao et al., 2021a; Bai et al., 2021). The lithofacies types developed in Well XKD-1 are very similar to those occurring in a series of profiles along outcrops (Huang et al., 2015; Zheng et al., 2020; Bai et al., 2021), and the lithofacies analysis suggests that the sedimentary environment is generally the tidal flat and lagoon environments.

The laminated dolostones at the bottom of the Xiaoerbulake Formation with dark-colored and continuous laminae reflect a restricted subtidal environment with low water circulation, weak reduction, and low energy in the subtidal zone. Such laminae may be related to microbial induced precipitation of micrite. Thrombolite dolostone above the laminated dolostones is mainly composed of micrite and tiny pellets, which also indicate weak hydrodynamics during deposition. The formation of micrite

10.3389/feart.2022.1075941

TABLE 1 Major and minor elements results of the Xiaoerbulake Formation

Sample name	type	Na (μg/g)	Si (μg/g)	Ti (μg/g)	Mn (μg/g)	Fe (μg/g)	Sr (μg/g)	Zr (μg/g)	Ba (μg/g)
LT3-37-a	MC	218.74	3716.16	37.03	86.88	1734.64	1036.44	1.55	7.31
LT3-37-b	MC	126.95	5875.96	26.96	92.11	1632.92	1076.13	1.21	6.22
XKD1-8-a	CD	0.00	1259.53	0.65	129.85	21.76	20.67	0.00	0.08
XKD1-8-b	MD	89.70	1277.29	0.08	114.12	242.09	60.53	0.00	0.45
XKD1-11-a	CD	10.47	1562.98	0.86	134.84	57.13	20.88	0.00	0.00
XKD1-11-b	MD	367.39	1374.87	0.00	90.52	86.26	58.53	0.00	0.82
XKD1-11-c	MD	163.11	1657.48	1.05	113.70	115.67	39.90	0.06	1.26
XKD1-13-a	BC	0.00	1636.61	0.00	0.00	40.57	347.16	0.05	0.24
XKD1-13-b	MD	547.79	1391.59	1.22	81.96	61.67	79.15	0.06	1.59
XKD1-13-c	MD	262.99	1351.94	0.00	95.66	144.59	60.19	0.17	0.92
XKD1-13-d	CD	0.00	1401.40	0.99	167.41	131.48	14.88	0.00	0.05
XKD1-13-e	CD	0.00	1548.85	0.95	148.03	68.62	13.56	0.07	0.05
XKD1-43-a	CD	7.12	1622.31	1.93	99.79	5.08	20.35	0.00	0.00
XKD1-43-b	CD	0.00	1460.73	0.48	160.49	164.24	17.38	0.07	0.00
XKD1-43-c	CD	0.00	1711.18	2.13	99.45	16.34	17.53	0.00	0.00
XKD1-43-d	BC	4.24	1434.43	0.00	0.14	12.03	121.74	0.05	0.07
XKD1-59-a	CD	4.36	1486.06	0.00	109.26	4.43	14.72	0.00	0.19
XKD1-59-b	CD	9.91	1660.69	0.00	108.07	14.90	15.89	0.00	0.04
XKD1-59-c	CD	7.81	1525.55	0.64	105.74	0.00	17.81	0.00	0.04
XKD1-59-d	MD	199.60	1700.55	0.22	116.57	88.97	42.72	0.06	0.46

TABLE 2 REE + Y results of the Xiaoerbulake Formation.

Sample name	type	ΣREE (μg/g)	Prn/Ybn	Ce/Ce*	Eu/Eu*	Y/Ho
LT3-37-a	MC	1.910	1.379	1.04	0.87	165.28
LT3-37-b	MC	2.183	1.102	0.96	1.21	52.19
XKD1-8-a	CD	0.268	0.484	0.99	2.21	71.89
XKD1-8-b	MD	0.170	0.373	0.49	1.02	21.70
XKD1-11-a	CD	0.543	0.638	0.78	1.25	49.09
XKD1-11-b	MD	0.160	0.461	0.65		41.61
XKD1-11-c	MD	0.165	2.043	0.74		51.96
XKD1-13-a	BC	0.341	0.204	0.01	2.57	31.11
XKD1-13-b	MD	0.236	1.021	0.89	0.85	35.06
XKD1-13-c	MD	0.225	0.817	0.82	0.55	55.77
XKD1-13-d	CD	0.703	0.442	0.93	0.77	
XKD1-13-e	CD	0.924	1.074	0.91	0.62	26.20
XKD1-43-a	CD	0.431	0.842	1.03	1.13	37.23
XKD1-43-b	CD	0.610	0.972	1.03	0.83	
XKD1-43-c	CD	0.441	1.456	0.97	1.84	37.79
XKD1-43-d	BC	0.431	1.067	0.05	0.56	30.70
XKD1-59-a	CD	0.420	0.476	1.07	1.28	54.82
XKD1-59-b	CD	0.395	0.639	0.85	0.86	83.17
XKD1-59-c	CD	0.385	0.476	0.75	1.16	83.03
XKD1-59-d	MD	0.164	1.061	0.63	1.96	36.21

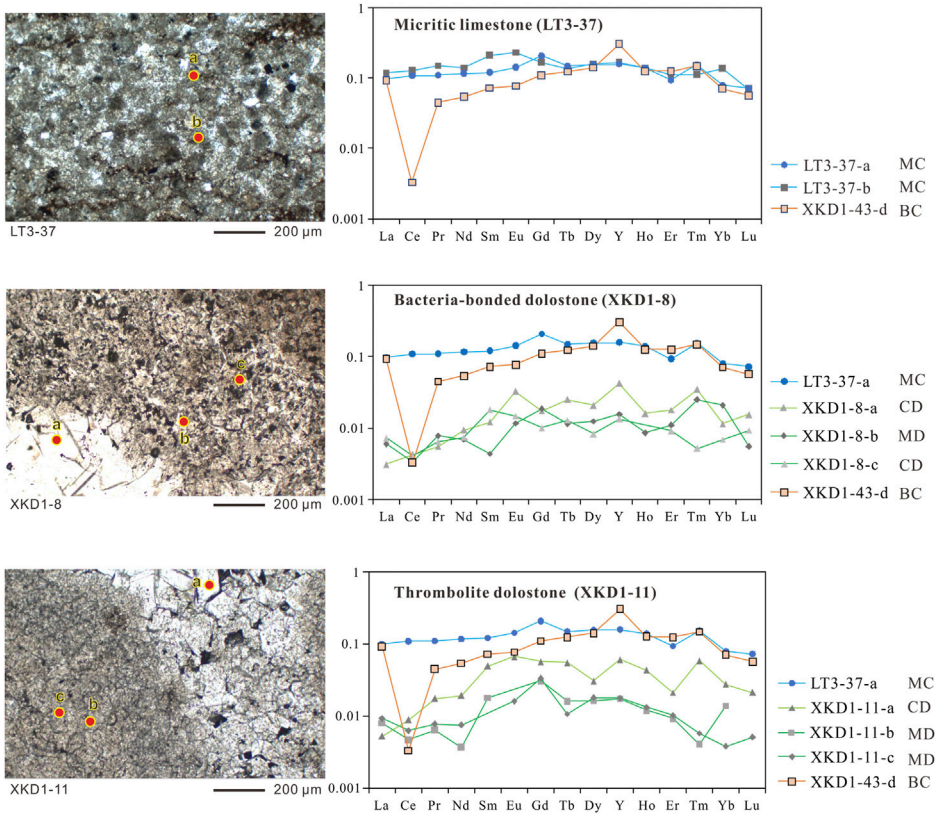

FIGURE 7
The REE+Y patterns of different types of dolomites (sampes LT3-37, XKD1-8, and XKD1-11) in the Xiaoerbulake Formation of the well XKD-1.

clots is usually attributed to the binding and trapping of microbial process in a low-energy subtidal zone below the wave base. Laminated and thrombolite dolostone are associated with the development of bacteria-bonded dolostone. This three lithofacies share similar sedimentary environments, and yet the bacteria-bonded dolostone has a shallower water depth, which is more suitable for the growth of microbial mats. Grain dolostones are mainly characterized by peloids and bacteria-bonded structures, reflecting medium-energy environment where grains were trapped and bond by microbial mats. The depositional environment was interpreted to be the lower intertidal zone to the upper subtidal zone above the wave base. The sedimentary environment changes from restricted subtidal lagoon to microbial mound in shallow subtidal zone, then to intertidal zone, which represents a complete upward-shallowing sequence. Such sedimentary sequence was consistent with the middle and lower part of the formation in both wells and outcrops in the northwestern Tarim Basin (Zheng et al., 2020; Bai et al., 2021). The uppermost part of the formation in the Well XKD-1 is dominant by breccia dolostone that were then capped by Quaternary deposits, indicating intense denudation and weathering by thrust uplift. About 20–30 m strata of the Xiaoerbulake Formation in the Well XKD-1 were eroded comparing to the outcrops and wells nearby (Zheng et al., 2020; Bai et al., 2021).

6.2 Differentiated genesis of various dolostone

Carbon isotopes are, in most cases, related to microbial process, organic matter content, meteoric diagenesis, etc., and less related to burial diagenesis (Qing and Veizer, 1994; Peng et al., 2002; Gao et al., 2021c). The $\delta^{13}C$ of the Xiaoerbulake Formation overlap largely with the Cambrian seawater $\delta^{13}C$ estimated by Veizer et al. (1999); Montanez et al. (2000), indicating that they mainly recorded the carbon isotope composition of the Cambrian seawater. The bacteria-bonded and laminated dolostone of Well XKD-1 have the lowest $\delta^{13}C$ values (0.873‰–2.742‰ VPDB) among all samples. Comprehensive lithofacies analysis shows that the wide distribution range of $\delta^{13}C$ may be attributed to microbially-induced micrite precipitation, while the

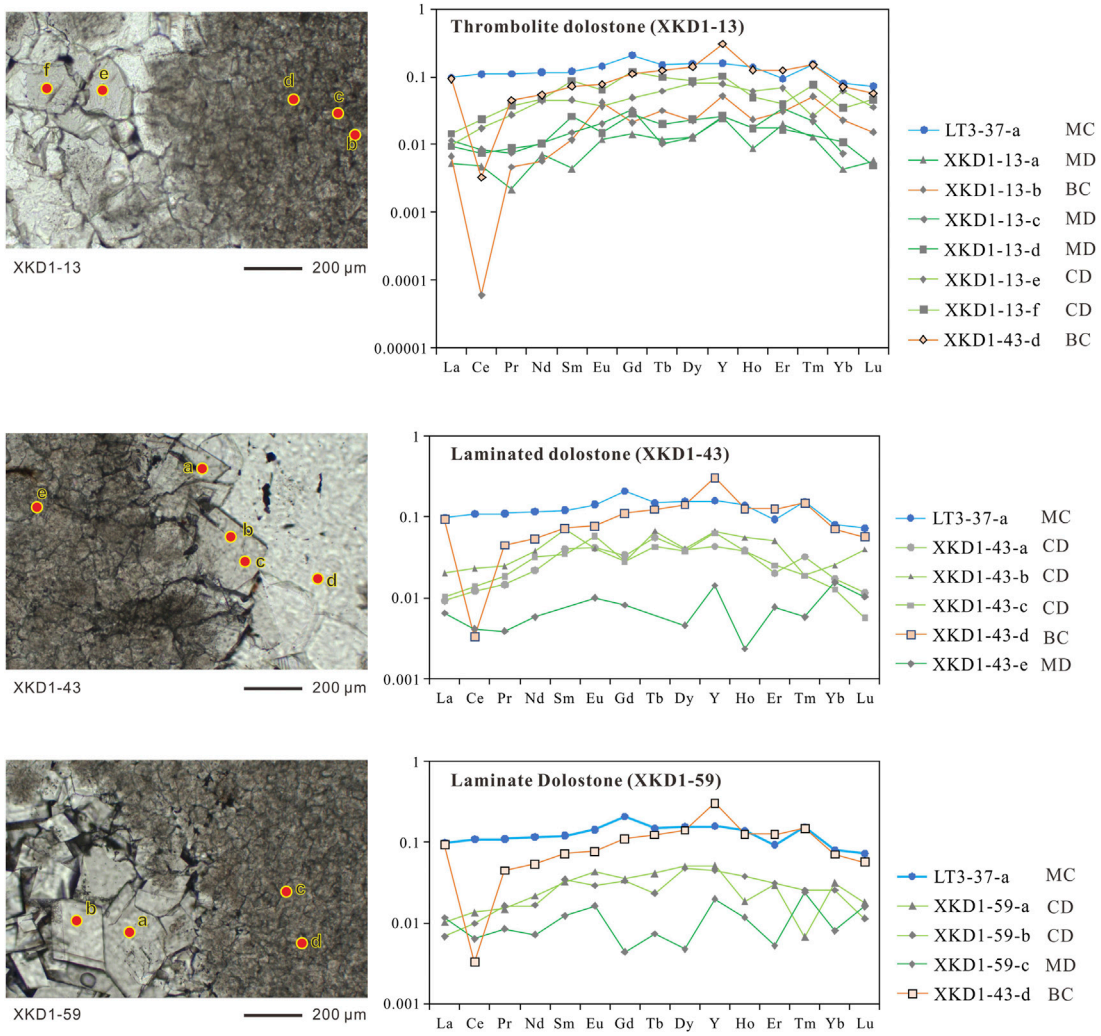

FIGURE 8
The patterns of REE+Y of different types of dolomites (XKD1-13, XKD1-43, and XKD1-59) in the Xiaoerbulake Formation of the well XKD-1.

extremely low $\delta^{13}C$ values are likely related to the early diagenesis by meteoric diagenesis (Fan et al., 2011; Gao et al., 2021c). In terms of $\delta^{18}O$ values, the thrombolite dolostone and grain dolostone both present significantly depleted $\delta^{18}O$, which are lower than the Cambrian seawater $\delta^{18}O$ estimated by Veizer et al. (1999); Montanez et al. (2000). The depletion of oxygen isotope can be caused by burial diagenesis and durative dolomitization (Melim and Scholle, 2002; Azomani et al., 2013; Ren et al., 2019). In contrast, the laminated dolostone and bacteria-bonded dolostone have greater $\delta^{18}O$ value which are closer to the Cambrian seawater $\delta^{18}O$ (Veizer et al., 1999; Montañez et al., 2000), indicating that they were less modified during burial diagenesis, and in other words, their dolomitization process completed during early diagenetic stage.

The scatter plots of strontium ratios and oxygen isotope values (Figure 5) illustrate that for most samples, the $^{87}Sr/^{86}Sr$ are very close to those of the Cambrian seawater (0.7085–0.7095) (Denison et al., 1998). This indicates that despite the variance in lithofacies, sedimentary structure, and diagenetic modification, most of the $^{87}Sr/^{86}Sr$ ratios retained in the dolostone were from seawater. However, two samples of laminated dolostone present slightly higher $^{87}Sr/^{86}Sr$ ratios than that Cambrian seawater, which may be caused by the influx of hyper-saline brine or meteoric water (Denison et al., 1998; Huang et al., 2007; Ngia et al., 2019a; Ngia et al., 2019b). Although the grain dolostones and thrombolite grainstones are subjected to intensive diagenetic alterations, resulting in strong depletion of $\delta^{18}O$, the dolomitization fluids were also marine origin.

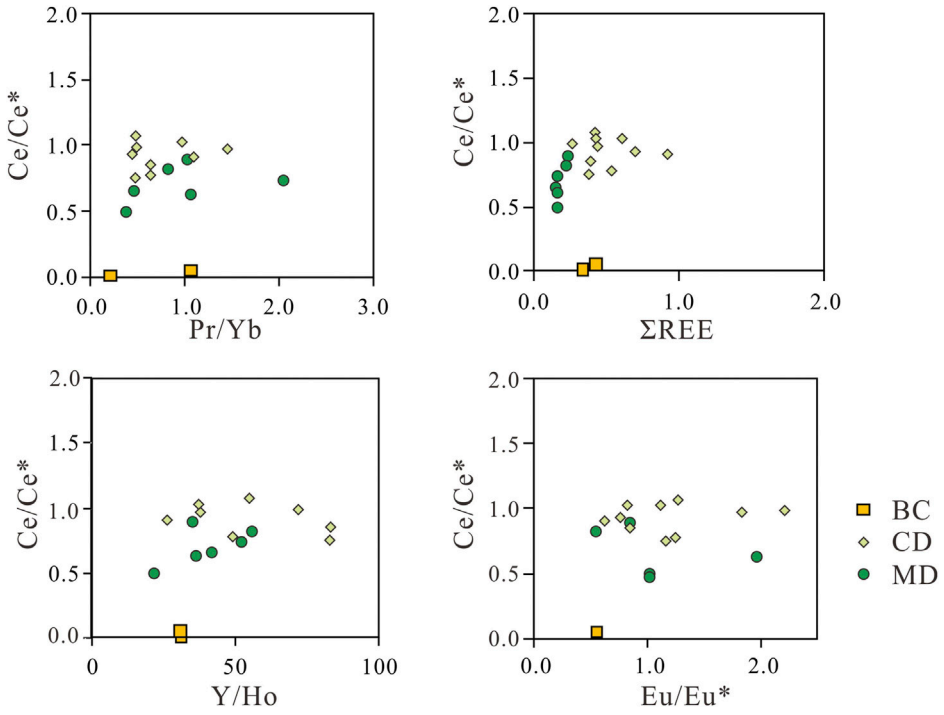

FIGURE 9
The cross-plots of rare Earth element parameters of different types of dolomites in the Xiaoerbulake Formation of the well XKD-1.

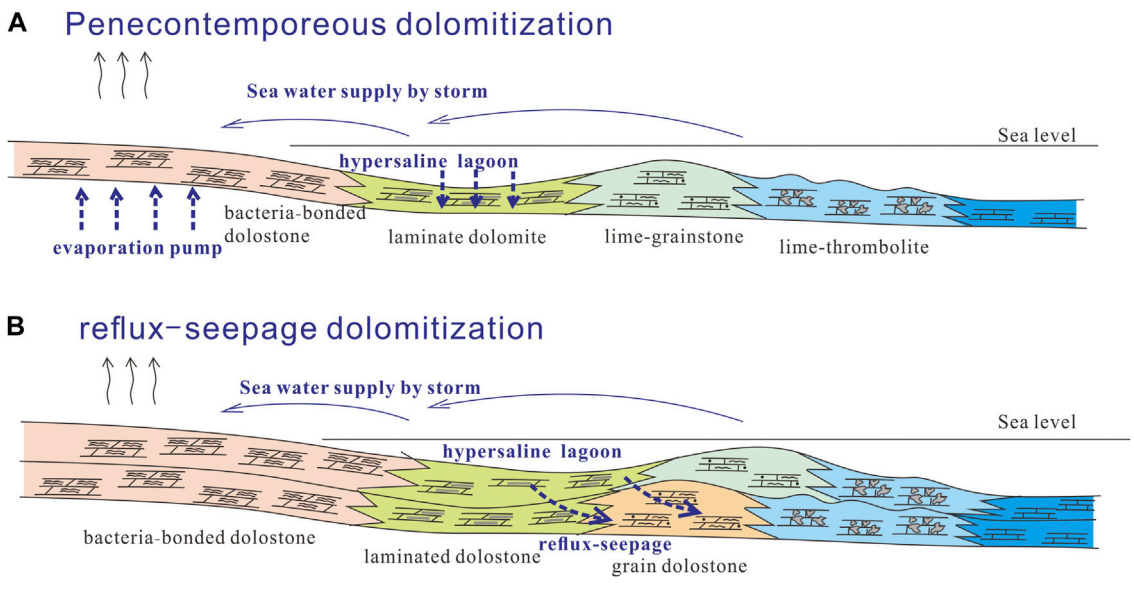

FIGURE 10
The dolomitization models for the Xiaoerbulake Formation in the well XKD-1 in the northwest of the Tarim Basin. **(A)** Penecontemporeous dolomitization for the bacteria-bonded dolostone and laminate dolomite. **(B)** Reflux-seepage dolomitization for grain dolostone and thrombolite dolostone.

6.3 Dolomite genesis and dolomitization model

Dolostones in Well XKD-1 are featured by abundant developed matrix dolomites. The contents of cement dolomite in grain dolostone and thrombolite dolostone are slightly higher than in laminated and bacteria-bonded dolostone. The content and covariance of Fe and Mn can be used to indicate diagenesis. Reducing conditions are favorable for Fe and Mn iron to enter carbonate crystals (Huang et al., 2007; Wang et al., 2021), and Fe and Mn may be positively correlated with each other as diagenesis intensifies with the increasing burial depth (Brand and Veizer, 1980; Huang 1990; Budd, 1997). As is shown in Figure 6, there is a weak positive correlation between Fe and Mn in matrix dolomite, but a strong positive correlation between Fe and Mn in cement dolomite. (Figure 6). Therefore, it can be inferred that the matrix dolomite experienced limited burial diagenesis, while the cement dolomite experienced continuous burial diagenesis.

The MD samples have significantly higher Na and slightly higher Sr than the CD shown in Figure 6. Seawater is abundant in Sr and Na, and high Na contents are indicative of hyper-saline water and low Na contents generally relate to diagenetic fluids (He et al., 2014; Ren et al., 2016). Moreover, Sr values generally decreases during dolomitization (Chen et al., 2008; Su et al., 2011; Ren et al., 2016). This therefore implies that MD were formed by seawater with slightly higher salinity, while the CD were precipitated from diagenetic fluids with low Na values under burial conditions. Compared with MC, MD have slightly higher Na values, which indicates that MD were mainly formed brine having a bit higher salinity than seawater. In addition, the strontium content of MD is greatly lower than that of MC, which indicates a significant depletion in Sr content during dolomitization process. Moreover, CD and pore-filling BC have similar Na contents, which proves that these carbonate cements were precipitated from diagenetic fluids with low-Na content under burial conditions. The scatter plots of Sr versus Ba (Figure 6) shows that CD and BC are characterized by low Ba content. Such low Ba content is mainly attributed to seawater, which means that with progress in burial diagenesis, Ba concentration of diagenetic fluids reduce constantly during the precipitation of BC and CD.

As for the REE + Y partition pattern, MC has the highest ΣREE and shows generally flat outline. These features were interptreted to be affected by the influx of terrigenous clastic minerals and thus the MC cannot represent original seawater (Van Kranendonk et al., 2003; Nothdurft et al., 2004; Kamber et al., 2014). MD display depleted LREE, negative Ce anomaly and an average Y/HO ratio of 40.38, which indicates that matrix dolomite may records the REE partition pattern of seawater during deposition (Webb and Kamber, 2000; Van Kranendonk et al., 2003; Bolhar et al., 2004; Shields and Webb, 2004; Zhang et al., 2016). During diagenesis, although most dolomite can retain the REE assemblage pattern of the original sedimentary period (Banner et al., 1988; Webb and Kamber, 2000; Nothdurft et al., 2004), the HREE may be preferentially removed from carbonates. Some samples of matrix dolomite present slight lower HREE, indicating that diagenesis affected the REE contents of matrix dolomite to some extent (Haley et al., 2004; Bayon et al., 2011). The positive Eu anomaly of carbonate rock is typically effective indicator of hydrothermal fluids, and the temperature of such fluids is slightly higher than that of the diagenetic environment (Alexander et al., 2008; Yu et al., 2016; Khelen et al., 2017; Sylvestre et al., 2017). Some samples show positive Eu anomalies (Figure 7), suggesting that they were precipitated by hydrothermal fluids. The REE patterns of most samples of CD show largely depleted HREE, which, together with the low Prn/Ybn of CD results in a hat-shaped outline. These characteristics represent depletion of both HREE and LREE, and enrichment of MREE in the burial environment (Haley et al., 2004; Kim et al., 2012; Surya Prakash et al., 2012). Meanwhile, the Ce anomaly of CD display a weak negative anomaly (0.75–1.07, average 0.93), which indicates a reducing diagenetic environment (German and Elderfield, 1990; Byrne and Sholkovitz, 1996; Bolhar and Van Kranendonk, 2007; Komiya et al., 2008; Ling et al., 2013). Eu anomaly of CD display both negative and positive anomalies, which is similar to matrix dolomite, suggesting that their parent fluids inherited the signature of hydrothermal fluids or were affected by high-temperature fluid activity and yet no extensive hydrothermal dolomitization.

The dolomitization process of the Lower Cambrian Xiaoerbulake Formation can be summarized in a dolomitization model develop at restricted platform (Figure 10). Matrix dolomites are characterized by high contents of Sr, Na, and Ba, low content of Fe and Mn, and seawater-like REE pattern, which indicates that MD was mainly formed during early diagenesis before burial through penecontemporaneous dolomitization by seawater or hyper-saline seawater (Figure 10). Some samples of MD show a slight depletion of HREE, reflecting limited diagenetic modification. Cement dolomites are characterized by low contents of Sr, Na, and Ba, and high contents Fe and Mn. Their REE patterns are similar to matrix dolomite, but with negative Ce anomaly, and enriched MREE. These features indicate that CD was formed in burial diagenetic environment under reducing conditions (Figure 10). The REE partition patterns of CD still represent marine fluids, and thus they were probably formed by the seepage-reflux dolomitization. In the process of continuous infiltration and dolomitization, Sr and Na are continuously consumed. During the burial diagenesis, Fe and Mn gradually accumulate in dolomite. Meanwhile, LREE and HREE are lost and HREE is relatively enriched. The reducing burial environment also diluted the negative anomaly of Ce in the CD samples. In addition, some samples of MD and CD have positive Eu anomalies, indicating local hydrothermal influence.

7 Conclusion

The Lower Cambrian Xiaoerbulake Formation in the Tarim Basin is mainly composed of laminated dolostone, thrombolite dolostone, bacteria-bonded dolostone, and grain dolostone that are deposited in a restricted platform.

Two types of dolomites are identified in the formation which are matrix dolomite and cement dolomite. The former is the primary dolomite type of laminated and bacteria-bonded dolostone, while the latter mainly occurs in pores developed in grain dolostone and thrombolite dolostone.

The carbon and oxygen isotopic values show that grain dolostone and thrombolite dolostone underwent more intense diagenetic modification than laminated dolostone and bacteria-bonded dolostone, which indicates that dolomitization of the latter two types of dolomites occurs during the early diagenesis. The strontium isotope ratios indicate that the dolomitization fluids were seawater or marine fluids.

Matrix dolomites were formed by penecontemporaneous dolomitization in seawater or hyper-saline seawater at early diagenesis stage, while cement dolomites were precipitated from seawater-origin fluids during sustained burial environment through seepage-reflux dolomitization process. Both types of dolomites are partially affected by hydrothermal fluids.

Data availability statement

The original contributions presented in the study are included in the article/supplementary material, further inquiries can be directed to the corresponding author.

Author contributions

HZ, DG, and LH contributed as the major authors of the article. All other authors listed have made a substantial, direct, and intellectual contribution to the work and approved it for publication.

Funding

This study was jointly funded by China National Petroleum Corporation Scientific Research and Technology Development Project (Grant No. 2021DJ05), and the National Natural Science Foundation of China (Grant No. 41502104).

Conflict of interest

Authors HZ, LH, GZ, TZ, JL, XZ, RX, and SW were employed by the company PetroChina.

The remaining authors declare that the research was conducted in the absence of any commercial or financial relationships that could be construed as a potential conflict of interest.

Publisher's note

All claims expressed in this article are solely those of the authors and do not necessarily represent those of their affiliated organizations, or those of the publisher, the editors and the reviewers. Any product that may be evaluated in this article, or claim that may be made by its manufacturer, is not guaranteed or endorsed by the publisher.

References

Alexander, B. W., Bau, M., Andersson, P., and Dulski, P. (2008). Continentally-derived solutes in shallow Archean seawater: Rare Earth element and Nd isotope evidence in iron formation from the 2.9 Ga Pongola Supergroup, South Africa. *Geochimica Cosmochimica Acta* 72 (2), 378–394. doi:10.1016/j.gca.2007.10.028

Azomani, E., Azmy, K., Blamey, N., Brand, U., and Al-Aasm, I. (2013). Origin of Lower Ordovician dolomites in eastern Laurentia: Controls on porosity and implications from geochemistry. *Mar. Petroleum Geol.* 40, 99–114. doi:10.1016/j.marpetgeo.2012.10.007

Bai, Y., Li, J. Z., Liu, W., Xv, Z. H., Xv, W. L., Li, X., et al. (2021). Characteristics and multiple dolomitization mode of the Lower Cambrian dolomite reservoir, northwestern Tarim Basin. *Acta Pet. Sin.* 42 (9), 1174–1191. (in Chinese with English abstract). doi:10.7623/syxb202109005

Banner, J. L., Hanson, G. N., and Meyers, W. J. (1988). Rare Earth element and Nd isotopic variations in regionally extensive dolomites from the Burlington-Keokuk Formation (Mississippian): Implications for REE mobility during carbonate diagenesis. *J. Sediment. Petrology* 58 (3), 415–432.

Bayon, G., Birot, D., Ruffine, L., Caprais, J. C., Ponzevera, E., Bollinger, C., et al. (2011). Evidence for intense REE scavenging at cold seeps from the Niger Delta margin. *Earth Planet. Sci. Lett.* 312 (3-4), 443–452. doi:10.1016/j.epsl.2011.10.008

Bolhar, R., Kambera, B. S., Moorbathb, S., Fedoc, M., and Whitehoused, M. J. (2004). Characterisation of early Archaean chemical sediments by trace element signatures. *Earth Planet. Sci. Lett.* 222 (1), 43–60. doi:10.1016/j.epsl.2004.02.016

Bolhar, R., and Van Kranendonk, M. J. (2007). A non-marine depositional setting for the northern Fortescue Group, Pilbara Craton, inferred from trace element geochemistry of stromatolitic carbonates. *Precambrian Res.* 155 (3-4), 229–250. doi:10.1016/j.precamres.2007.02.002

Brand, U., and Veizer, J. (1980). Chemical diagenesis of a multicomponent carbonate system: 1. Trace elements. *J. Sediment. Petrology* 50, 1219–1236.

Budd, D. A. (1997). Cenozoic dolomites of carbonate islands: Their attributes and origin. *Earth-Science Rev.* 42 (1/2), 1–47. doi:10.1016/s0012-8252(96)00051-7

Byrne, R. H., and Sholkovitz, E. R. (1996). *Handbook on the physics and chemistry of the rare earths.* Amsterdam: Elsevier, 497–593.

Chen, Y. Q., Zhou, X. Y., Zhao, K. D., Yang, W. J., Dong, C. Y., and Zhu, C. J. (2008). Geochemical research on straticulate dolostone and spatulate dolostone in lower ordovician strata of well tazhong-1, Tarim Basin. *Acta Geol. Sin.* 82 (6), 826–834. (in Chinese with English abstract). doi:10.3321/j.issn:0001-5717.2008.06.012

Denison, R. E., Koepnick, R. B., Burke, W. H., and Hetherington, E. A. (1998). Construction of the cambrian and ordovician seawater $^{87}Sr/^{86}Sr$ curve. *Chem. Geol.* 152 (3/4), 325–340. doi:10.1016/s0009-2541(98)00119-3

Fan, R., Deng, S. H., and Zhang, X. L. (2011). Global correlation of carbon isotope excursion through the Cambrian. *Sci. China. Earth Sci.* 41 (12), 1829–1839. (in Chinese with English abstract).

Gao, D., Hu, M. Y., Li, A. P., Yang, W., Xie, W. R., and Sun, C. Y. (2021a). High-frequency sequence and microfacies and their impacts on favorable reservoir of Longwangmiao Formation in central Sichuan Basin. *Earth Sci.* 46 (10), 3520–3534. (in Chinese with English abstract).

Gao, D., Lin, C., Huang, L., Hu, M., Ren, P., Sun, C. Y., et al. (2021b). Depositional facies and diagenesis of the lianglitage Formation in northwestern tazhong uplift, Tarim Basin, China: Implications for the Genesis of ultra-deep limestone reservoir. *Arab. J. Geosci.* 14, 750. doi:10.1007/s12517-021-07080-9

Gao, D., Wang, M. M., Tao, Y., Huang, L. L., Sun, C. Y., Huang, X. M., et al. (2021c). Control of sea level changes on high-frequency sequence and sedimentary evolution of Lianglitage Formation in the Tazhong Area. *Geol. China*. (in Chinese with English abstract)

German, C. R., and Elderfield, H. (1990). Application of the Ce anomaly as a paleoredox indicator: The ground rules. *Paleoceanography* 5 (5), 823–833. doi:10.1029/pa005i005p00823

Guan, S. W., Wu, L., Ren, R., Zhu, G. Y., Peng, Z. Q., Zhao, W. T., et al. (2018). Distribution and petroleum prospect of Precambrian rifts in the main cratons, China. *Acta Pet. Sin.* 38 (1), 9–22. (in Chinese with English abstract).

Haley, B. A., Klinkhammer, G. P., and McManus, J. (2004). Rare Earth elements in pore waters of marine sediments. *Geochimica Cosmochimica Acta* 68 (6), 1265–1279. doi:10.1016/j.gca.2003.09.012

He, X. Y., Shou, J. F., Shen, A. J., Wu, X. N., Wang, Y. S., Hu, Y. Y., et al. (2014). Geochemical characteristics and origin of dolomite: A case study from the middle assemblage of majiagou formation member 5 of the west of jingbian gas field, ordos basin, north China. *Petroleum Explor. Dev.* 41 (3), 375–384. (in Chinese with English abstract).

Hu, Z. C., Zhang, W., Liu, Y. S., Gao, S., Li, M., Zong, K. Q., et al. (2015). Wave" signal-smoothing and mercury-removing device for laser ablation quadrupole and multiple collector ICPMS Analysis: Application to Lead Isotope Analysis. *Anal. Chem.* 87 (2), 1152–1157. doi:10.1021/ac503749k

Huang, Q. Y., Liu, W., Zhang, Y. Q., Shi, S. Y., and Wang, K. (2015). Progress of research on dolomitization and dolomite reservoir. *Adv. Earth Sci.* 30 (5), 539–551. (in Chinese with English abstract). doi:10.11867/j.issn.1001-8166.2015.05.0539

Huang, S. J. (1990). Cathodoluminescence and diagenetic alteration of marine carbonate minerals. *Sediment. Geol. Tethyan Geol.* 4, 9–15. (in Chinese with English abstract).

Huang, S. J., Liu, S. G., Li, G. R., Zhang, M., and Wu, W. H. (2014). Protective immunity against HEV. *Curr. Opin. Virol.* 31 (1), 1–6. (in Chinese with English abstract). doi:10.1016/j.coviro.2013.10.003

Huang, S. J., Qing, H. R., Hu, Z. W., Zou, M. L., Feng, W. L., Wang, C. M., et al. (2007). Closed-system dolomitization and the significance for petroleum and economic geology: An example from Feixianguan carbonates, Triassic, NE Sichuan basin of China. *Acta Petrol. Sin.* 23 (11), 2955–2962. (in Chinese with English abstract).

Kamber, B. S., Webb, G. E., and Gallagher, M. (2014). The rare Earth element signal in Archaean microbial carbonate: Information on ocean redox and biogenicity. *J. Geol. Soc. Lond.* 171 (6), 745–763. doi:10.1144/jgs2013-110

Khelen, A. C., Manikyamba, C., Ganguly, S., Singh, T. D., Subramanyam, K. S. V., Ahmad, S. M., et al. (2017). Geochemical and stable isotope signatures of Proterozoic stromatolitic carbonates from the Vempalle and Tadpatri Formations, Cuddapah Supergroup, India: Implications on paleoenvironment and depositional conditions. *Precambrian Res.* 298, 365–384. doi:10.1016/j.precamres.2017.05.021

Kim, J. H., Torres, M. E., Haley, B. A., Kastner, M., Pohlman, J. W., Riedel, M., et al. (2012). The effect of diagenesis and fluid migration on rare Earth element distribution in pore fluids of the northern Cascadia accretionary margin. *Chem. Geol.* 291 (6), 152–165. doi:10.1016/j.chemgeo.2011.10.010

Komiya, T., Hirata, T., Kitajima, K., Yamamoto, S., Shibuya, T., Sawaki, Y., et al. (2008). Evolution of the composition of seawater through geologic time, and its influence on the evolution of life. *Gondwana Res.* 14 (1-2), 159–174. doi:10.1016/j.gr.2007.10.006

Li, B., Peng, J., Yang, S. J., Xia, Q. S., Xv, Q. Q., and Hao, R. Q. (2017). Genetic model and characteristics of the cambrian shorebulake reservoir in Bachu area, Tarim Basin. *Petroleum Geol. Exp.* 39 (6), 797–804. (in Chinese with English abstract). doi:10.11781/sysydz201706797

Ling, H. F., Chen, X., Li, D., Wang, D., Shields-Zhou, G. A., and Zhu, M. (2013). Cerium anomaly variations in Ediacaran-earliest Cambrian carbonates from the Yangtze Gorges area, South China: Implications for oxygenation of coeval shallow seawater. *Precambrian Res.* 225, 110–127. doi:10.1016/j.precamres.2011.10.011

Liu, D. W., Cai, C. F., Gu, Y. J., Jiang, L., Peng, Y. Y., Yu, R., et al. (2020). Multi-stage dolomitization process of deep burial dolostones and its influence on pore evolution: A case study of longwangmiao formation in the lower cambrian of central sichuan basin. *J. China Univ. Min. Technol.* 49 (6), 1150–1165. (in Chinese with English abstract). doi:10.13247/j.cnki.jcumt.001181

Liu, Y. S., Hu, Z. C., Gao, S., Günther, D., Xu, J., Gao, C. G., et al. (2008). *In situ* analysis of major and trace elements of anhydrous minerals by LA-ICP-MS without applying an internal standard. *Chem. Geol.* 257 (1-2), 34–43. doi:10.1016/j.chemgeo.2008.08.004

Melim, L. A., and Scholle, P. A. (2002). Dolomitization of the capitan formation forereef facies (permian, west Texas and new Mexico): Seepage reflux revisited. *Sedimentology* 49, 1207–1227. doi:10.1046/j.1365-3091.2002.00492.x

Montañez, I. P., Osleger, D. A., Banner, J. L., Mack, L. E., and Musgrove, M. (2000). Evolution of the Sr and C isotope composition of Cambrian oceans. *GSA Today* 10, 1–7.

Ngia, N. R., Hu, M., Gao, D., Hu, Z., and Sun, C. Y. (2019a). Application of stable strontium isotope geochemistry and fluid inclusion microthermometry to studies of dolomitization of the deeply buried cambrian carbonate successions in west-central Tarim Basin, NW China. *J. Earth Sci.* 30, 176–193. doi:10.1007/s12583-017-0954-y

Ngia, N. R., Hu, M., and Gao, D. (2019b). Tectonic and geothermal controls on dolomitization and dolomitizing fluid flows in the cambrian-lower ordovician carbonate successions in the western and central Tarim Basin, nw China. *J. Asian Earth Sci.* 172, 359–382. doi:10.1016/j.jseaes.2018.09.020

Nothdurft, L. D., Webb, G. E., and Kamber, B. S. (2004). Rare Earth element geochemistry of Late Devonian reefal carbonates, Canning Basin, Western Australia: Confirmation of a seawater REE proxy in ancient limestones. *Geochimica Cosmochimica Acta* 68 (2), 263–283. doi:10.1016/s0016-7037(03)00422-8

Ouyang, S., Lyu, X., Xue, N., Li, F., and Wang, R. (2022). Paleoenvironmental characteristics and source rock development model of the early-middle cambrian: A case of the keping-bachu area in the Tarim Basin. *J. China Univ. Min. Technol.* 51 (2), 293–310. (in Chinese with English abstract). doi:10.13247/j.cnki.jcumt.001335

Peng, S., He, H., Shao, L., Shi, Z., and Gao, Y. (2002). Carbon isotopic compositions of the Cambrian-Ordovician carbonates in Tarim Basin. *J. China Univ. Min. Technol.* 31 (4), 353–357. (in Chinese with English abstract). doi:10.3321/j.issn:1000-1964.2002.04.006

Qing, H., and Veizer, J. (1994). Oxygen and carbon isotopic composition of ordovician brachiopods: implications for coeval seawater. *Geochimica et Cosmochimica Acta.* 58 (20), 4429–4442. doi:10.1016/0016-7037(94)90345-x

Ren, R., Guan, S. W., Wu, L., and Zhu, G. Y. (2017). The north-south differentiation characteristic and its enlightenment on oil-gas exploration of the Neoproterozoic rift basin, Tarim Basin. *Acta Pet. Sin.* 38 (3), 255–266. (in Chinese with English abstract). doi:10.7623/syxb201703002

Ren, Y., Zhong, D., Gao, C., Sun, H., Peng, H., Zheng, X., et al. (2019). Origin of dolomite of the lower cambrian longwangmiao formation, eastern sichuan basin, China. *Carbonates Evaporites* 34 (3), 471–490. doi:10.1007/s13146-017-0409-7

Ren, Y., Zhong, D. K., Gao, C. L., Yang, X. Q., Xie, R., Li, Z. P., et al. (2016). Geochemical characteristics, Genesis and hydrocarbon significance of dolomite in the cambrian longwangmiao formation, eastern sichuan basin. *Acta Pet. Sin.* 37 (9), 1102–1115. (in Chinese with English abstract). doi:10.7623/syxb201609004

Shields, G. A., and Webb, G. E. (2004). Has the REE composition of seawater changed over geological time? *Chem. Geol.* 204 (1-2), 103–107. doi:10.1016/j.chemgeo.2003.09.010

Song, J. M., Luo, P., Yang, S. S., Yang, D., Zhou, C. M., Li, P. W., et al. (2014). Reservoirs of lower cambrian microbial carbonates, Tarim Basin, NW China. *Petroleum Explor. Dev.* 41 (4), 449–459. (in Chinese with English abstract). doi:10.1016/s1876-3804(14)60051-3

Song, Y. F., Chen, D. Z., Guo, C., and Zhou, X. C. (2020). Depositional characteristics of microbial carbonates from the lower xiaoerbulak Formation in the Xiaoerbulake section, Tarim Basin. *Acta Sedimentol. Sin.* 38 (1), 55–63. (in Chinese with English abstract). doi:10.14027/j.issn.1000-0550.2019.024

Su, Z. T., Chen, H. D., Xv, F. Y., Wei, L. B., and Li, J. (2011). Geochemistry and dolomitization mechanism of majiagou dolomites in ordovician, ordos, chin. *Acta Petrol. Sin.* 27 (8), 2230–2238. (in Chinese with English abstract).

Surya Prakash, L., Ray, D., Paropkari, A. L., Mudholkar, A. V., Satyanarayanan, M., Sreenivas, B., et al. (2012). Distribution of REEs and yttrium among major geochemical phases of marine Fe-Mn-oxides: Comparative study between hydrogenous and hydrothermal deposits. *Chem. Geol.* 312-313, 127–137. doi:10.1016/j.chemgeo.2012.03.024

Sylvestre, G., Evine Laure, N. T., Gus Djibril, K. N., Arlette, D. S., Cyriel, M., Timoléon, N., et al. (2017). A mixed seawater and hydrothermal origin of superior-type banded iron formation (BIF)-hosted Kouambo iron deposit, Palaeoproterozoic Nyong series, Southwestern Cameroon: Constraints from petrography and geochemistry. *Ore Geol. Rev.* 80, 860–875. doi:10.1016/j.oregeorev.2016.08.021

Van Kranendonk, M. J., Webb, G. E., and Kamber, B. S. (2003). Geological and trace element evidence for a marine sedimentary environment of deposition and biogenicity of 3.45 Ga stromatolitic carbonates in the Pilbara Craton, and support for a reducing Archaean ocean. *Geobiology* 1 (2), 91–108. doi:10.1046/j.1472-4669.2003.00014.x

Veizer, J., Ala, D., Azmy, K., Bruckschen, P., Buhl, D., Bruhn, F., et al. (1999). $^{87}Sr/^{86}Sr$, $\delta^{13}S$ and $\delta^{18}O$ evolution of phanerozoic seawater. *Chem. Geol.* 161 (1), 59–88. doi:10.1016/s0009-2541(99)00081-9

Wang, Y., Shi, Z. J., Qing, H. R., Tian, Y., and Gong, X. (2021). Petrological characteristics, geochemical characteristics, and dolomite model of the lower cambrian longwangmiao Formation in the periphery of the sichuan basin, China. *J. Petroleum Sci. Eng.* 202, 108432–108517. doi:10.1016/j.petrol.2021.108432

Wang, Z. M., Xie, H. W., Chen, Y. Q., Qi, Y. M., and Zhang, K. (2014). Discovery and exploration of cambrian subsalt dolomite original hydrocarbon reservoir at zhongshen-1 well in Tarim Basin. *China Pet. Explor.* 19 (2), 1–13. (in Chinese with English abstract). doi:10.3969/j.issn.1672-7703.2014.02.001

Warren, J. (2000). Dolomite: Occurrence, evolution and economically important associations. *Earth-Science Rev.* 52, 1–81. doi:10.1016/s0012-8252(00)00022-2

Webb, G. E., and Kamber, B. S. (2000). Rare Earth elements inHolocene reefal microbialites: A new shallow seawater proxy. *Geochimica Cosmochimica Acta* 64 (9), 1557–1565. doi:10.1016/s0016-7037(99)00400-7

Wei, G. Q., Zhu, Y. J., Zheng, J. F., Yu, G., Ni, X. F., Yan, L., et al. (2021). Tectonic-lithofacies paleogeography, large-scale source-reservoir distribution and exploration zones of Cambrian subsalt formation, Tarim Basin, NW China. *Petroleum Explor. Dev.* 48 (6), 1289–1303. doi:10.1016/s1876-3804(21)60287-2

Yan, W., Wu, G. H., Zhang, Y. Q., Yang, G., Lou, H., and Wang, X. M. (2018). Sinian-cambrian tectonic framework in the Tarim Basin and its influences on the paleogeography of the early cambrian. *Geotect. Metallogenia* 42 (3), 455–466. (in Chinese with English abstract). doi:10.16539/j.ddgzyckx.2018.03.004

Yan, W., Zheng, J. F., Chen, Y. Q., Huang, L. L., Zhou, P., and Zhu, Y. J. (2017). Characteristics and Genesis of dolomite reservoir in the lower cambrian xiaoerblak formation, Tarim Basin. *Mar. Orig. Pet. Geol.* 22 (4), 35–43. (in Chinese with English abstract). doi:10.3969/j.issn.1672-9854.2017.04.005

Yang, H. J., Yu, S., Zhang, H. Z., Li, T. F., Fan, S., Cheng, B., et al. (2020). Geochemical characteristics of Lower Cambrian sources rocks from the deepest drilling of Well LT-1 and their significance to deep oil gas exploration of the Lower Paleozoic system in the Tarim Basin. *Geochimica* 49 (6), 593. (in Chinese with English abstract). doi:10.19700/j.0379-1726.2021.01.017

Yu, Z. H., Li, H. M., Li, M. X., and Zhai, S. K. (2016). Hydrothermal signature in the axial-sediments from the carlsberg ridge in the northwest Indian Ocean. *J. Mar. Syst.* 180, 173–181. doi:10.1016/j.jmarsys.2016.11.013

Zenger, D. H., Dunham, J. B., and Ethington, R. L. (1980). *Concepts and models of dolomitization*. Tulsa: SEPM Special Publications, 1–328.

Zhang, C. Y., Guan, S. W., Wu, L., Ren, R., and Xiong, L. Q. (2021). Geochemical characteristics and its paleo-environmental significance of the lower cambrian carbonate in the northwestern Tarim Basin: A case study of well shutan-1. *Bull. Geol. Sci. Technol.* 40 (5), 99–111. (in Chinese with English abstract). doi:10.19509/j.cnki.dzkq.2021.0508

Zhang, L., Algeo, T. J., Cao, L., Zhao, L., Chen, Z. Q., and Li, Z. (2016). Diagenetic uptake of rare Earth elements by conodont apatite. *Palaeogeogr. Palaeoclimatol. Palaeoecol.* 458, 176–197. doi:10.1016/j.palaeo.2015.10.049

Zheng, J. F., Huang, L. L., Yuan, W. F., Zhu, Y. J., and Qiao, Z. F. (2020). Geochemical features and its significance of sedimentary and diagenetic environment in the lower cambrian xiaoerblak Formation of keping area, Tarim Basin. *Nat. Gas. Geosci.* 31 (5), 698–709. (in Chinese with English abstract). doi:10.11764/j.issn.1672-1926.2020.04.008

Zhu, Y. J., Ni, X. F., Liu, L. L., Qiao, Z. F., Chen, Y. Q., and Zheng, J. F. (2019). Depositional differentiation and reservoir potential and distribution of ramp systems during postrift period: An example from the lower cambrian Xiaoerbulake Formation in the Tarim Basin, NW China. *Acta Sedimentol. Sin.* 37 (5), 1044–1057. (in Chinese with English abstract). doi:10.14027/j.issn.1000-0550.2019.006

Zong, K. Q., Klemd, R., Yuan, Y., He, Z. Y., Guo, J. L., Shi, X. L., et al. (2017). The assembly of Rodinia: The correlation of early Neoproterozoic (ca. 900 Ma) high-grade metamorphism and continental arc formation in the southern Beishan Orogen, southern Central Asian Orogenic Belt (CAOB). *Precambrian Res.* 290, 32–48. doi:10.1016/j.precamres.2016.12.010